

Effective Removal of Toxic Heavy Metal Ions from Aqueous Solution by CaCO₃ Microparticles

Rui Zhang · Joseph J. Richardson ·
Anthony F. Masters · Gyeongwon Yun · Kang Liang ·
Thomas Maschmeyer

Received: 10 December 2017 / Accepted: 21 March 2018
© Springer International Publishing AG, part of Springer Nature 2018

Abstract Heavy metals are a common contaminant in water supplies and pose a variety of serious health risks to nearby human populations. A promising approach to heavy metal decontamination is the sequestration of heavy metal ions in porous materials; however, current technologies involve materials which can be difficult to synthesize, are high-cost, or are themselves potentially toxic. Herein, we demonstrate that rapidly synthesized calcium carbonate (CaCO₃) microparticles can effectively remove high quantities of Pb²⁺, Cd²⁺, and Cu²⁺

ions (1869, 1320, and 1293 mg per gram of CaCO₃ microparticles, respectively) from aqueous media. The CaCO₃ microparticles were characterized with powder X-ray diffraction (XRD), scanning electron microscopy (SEM), high-resolution transmission electron microscopy (HRTEM), and Brunauer–Emmett–Teller (BET) N₂ sorption–desorption. It was found that the Ca²⁺ ions of the microparticles were replaced by the heavy metal ions, leading to partially recrystallized nanoparticles of new compositional phases such as cerussite (PbCO₃). The adsorption, surface dissolution/re-precipitation, and nucleation/crystal growth mechanisms were determined by investigating the Ca²⁺ released, along with the changes to particle morphology and crystal structure. Importantly, this study demonstrates that the porous CaCO₃ microparticles performed well in a system with multiple heavy metal ion species: 100% of Cu²⁺, 97.5% of Pb²⁺, and 37.0% Cd²⁺ were removed from an aqueous solution of all cations with initial individual metal concentrations of 50 mg/L and 1.5 g/L of CaCO₃ microparticles. At this concentration, the CaCO₃ microparticles significantly outperformed activated carbon. These results help to establish CaCO₃ microparticles as a promising low-cost and scalable technology for removing heavy metal ions from contaminated water.

Electronic supplementary material The online version of this article (<https://doi.org/10.1007/s11270-018-3787-0>) contains supplementary material, which is available to authorized users.

R. Zhang · A. F. Masters · T. Maschmeyer (✉)
Laboratory of Advanced Catalysis for Sustainability, School of
Chemistry, The University of Sydney, Sydney, NSW 2006,
Australia
e-mail: thomas.maschmeyer@sydney.edu.au

J. J. Richardson · G. Yun
Department of Chemical Engineering, The University of
Melbourne, Melbourne, VIC 3010, Australia

J. J. Richardson
Manufacturing, CSIRO, Clayton, VIC 3168, Australia

K. Liang
School of Chemical Engineering, The University of New South
Wales, Sydney, NSW 2006, Australia

K. Liang
Graduate School of Biomedical Engineering, The University of
New South Wales, Sydney, NSW 2006, Australia

Keywords Calcium carbonate · Porous microparticles ·
Heavy metal adsorption · Adsorption mechanisms

1 Introduction

Despite a considerable amount of research to find alternatives to heavy metals (commonly defined as metals both heavier than 5 g/cm^3 and toxic at low concentrations) (Ricco et al. 2015), they still find ever increasing usage in modern products, including batteries, pesticides, paints, and electronics. Consequently, the rising presence of heavy metal waste in the environment provides a potential and possibly increasing risk of prolonged health problems to humans and other living species. For example, lead poisoning can severely affect central nervous systems (Okoye et al. 2010); cadmium compounds are likely human carcinogens, long-term exposure may cause fragile bones, kidney damage, and even death (Boparai et al. 2011; Srivastava et al. 2006); symptoms of copper poisoning include nausea, vomiting, and death (Fu and Wang 2011). These problems are exacerbated by the fact that heavy metals are usually not easily removed from the biosphere but instead tend to accumulate in living organisms (Annadurai et al. 2003; Fu and Wang 2011; Reed and Matsumoto 1993), making the problem of heavy metal contamination more severe. Therefore, simple and effective treatments for water contaminated with heavy metals have received continuous attention (Fu and Wang 2011).

Existing methods for heavy metal removal from water include chemical precipitation (Charemtanyarak 1999; Matlock et al. 2002), ion exchange (Tavakoli et al. 2017; Wang et al. 2014), membrane filtration (Al-Rashdi et al. 2013; Blöcher et al. 2003), and adsorption (Celis et al. 2000; Ho et al. 1996). Among these technologies, adsorption is one of the most promising methods, as it is generally passive and relatively facile. Recently, several types of adsorbents have been reported for removing heavy metals from water, including carbon nanotubes (Stafiej and Pyrzynska 2007), activated carbon (Amuda et al. 2007; Kobya et al. 2005), zeolites (Erdem et al. 2004), metal-organic frameworks (MOFs) (Ricco et al. 2015), nanosized metal oxides (Hua et al. 2012; Wang et al. 2010a), and resins (Lin et al. 2000). Among these adsorbents (Table 1), nano-adsorbents such as carbon nanotubes, MOFs, or metal oxide nanomaterials show a high capacity for adsorbing metal ions from aqueous solution due to their high surface areas; however, these adsorbents can be expensive and difficult to prepare (Gupta et al. 2011). Therefore, there is a pressing need for

adsorbents that are cost-effective, abundant, easy to prepare, biocompatible, and capable of efficiently removing heavy metals, that is, adsorption that is fast and extensive.

Calcium carbonate (CaCO_3) is one of earth's most abundant (thus, low cost) materials. It is biocompatible and biodegradable, meeting all of the desirable criteria for an adsorbent for large-scale use. However, previous studies on adsorbing heavy metals, utilizing various polymorphs of CaCO_3 : calcite (Gamsjäger et al. 1984), aragonite (Godelitsas et al. 2003), vaterite (Mohammadifard and Amiri 2017), and amorphous CaCO_3 (Cai et al. 2010), unfortunately demonstrated that natural CaCO_3 has a low removal efficiency for heavy metal ions (Yavuz et al. 2007). Cai et al. prepared amorphous calcium carbonate nanoparticles ($\sim 40 \text{ nm}$) as adsorbents and demonstrated that the capacity to remove Cd^{2+} , Pb^{2+} , Cr^{3+} , Fe^{3+} , and Ni^{2+} ions was significantly improved, indicating that the heavy metal removal capacity increased as the surface area of the CaCO_3 particles increased (Cai et al. 2010). Thus, the removal capacity is likely to depend on the surface morphology and surface chemistry. Therefore, porous CaCO_3 microparticles could potentially be even better adsorbents because: (1) they have a still higher surface area; (2) they are easier to separate than solid nanoparticles after heavy metal adsorption, as they are much larger than nanoparticles, making them easy to separate by filtration/centrifugation; and (3) they can be prepared in scalable quantities in a straightforward and rapid manner. Although a previous study investigated the ability of porous CaCO_3 -maltose hybrid microparticles to sequester heavy metals and showed impressive removal capacity (Ma et al. 2012b), to the best of our knowledge, the investigation of heavy metal removal ability by porous, pure CaCO_3 microparticles has not yet been reported.

In this work, we demonstrate that porous CaCO_3 microparticles, which are easily prepared using a rapid precipitation approach, can efficiently remove large quantities of Cd^{2+} , Pb^{2+} , and Cu^{2+} and combinations of these ions together from water. Specifically, the CaCO_3 microparticles could adsorb more than 100% of their own weight in heavy metal ions (i.e., 187% for Pb^{2+} , 132% for Cd^{2+} , and 129% for Cu^{2+}). This unprecedented adsorption capacity is due to a replacement reaction where the calcium ions were replaced by the heavy metal ions—a reaction made more facile due to the porous nature of the nanoparticles. The mechanism of adsorption was studied by examining: the amount of

Table 1 Adsorption conditions and capacity of different adsorbents

Adsorbents	Adsorption conditions	Adsorption capacity
Activated carbon (Kobyta et al. 2005)	2 mg/mL adsorbents	33.57 mg/g of Cd ²⁺
	48 h	22.85 mg/g of Pb ²⁺
		24.21 mg/g of Cu ²⁺
Zeolite (Erdem et al. 2004)	20 mg/mL adsorbents	3.5 mg/g of Cu ²⁺
MOF (Ricco et al. 2015)	5.5 h	
	6.7 mg/mL adsorbents	492.4 mg/g of Pb ²⁺
Nanosized metal oxides (Wang et al. 2010a)	24 h	
	0.5 mg/mL adsorbents	> 1600 mg/g of Cu ²⁺
Resin (Lin et al. 2000)	10 h	
	2 mg/mL adsorbents	92.5 mg/g of Cu ²⁺
This study	24 h	
	0.5 mg/mL adsorbents	1869 mg/mL of Pb ²⁺
	6 h	1320 mg/mL of Cd ²⁺
		1293 mg/mL of Cu ²⁺

Ca²⁺ released into the supernatant; the pH differences between the initial metal ion solution and the supernatant after the heavy metals had been adsorbed; the particles' morphology deduced by scanning electron microscopy (SEM) and high-resolution transmission electron microscopy (HRTEM); and the structural details of the metal compounds formed determined by using X-ray diffraction (XRD).

2 Materials and Methods

2.1 Chemicals

All chemicals were of analytical grade and used as received without any further purification. Anhydrous calcium chloride, anhydrous sodium carbonate, and anhydrous lead nitrate and nitric acid (69%, w/w) were purchased from ThermoFisher Scientific, Australia. Cadmium nitrate tetrahydrate, copper nitrate trihydrate, and activated carbon were purchased from Merck, Australia. Polystyrene sulfonate sodium (Mw = 70,000) was purchased from Sigma-Aldrich, Australia.

2.2 CaCO₃ Microparticle Formation

CaCO₃ microparticles were prepared following Richardson et al.'s method (Richardson et al. 2015). After particle formation, the particles were freeze-dried and stored in a sealed container at room temperature.

2.3 Characterization of the CaCO₃ Microparticles

The size and morphology of the CaCO₃ microparticles were determined via scanning electron microscopy (SEM) (Zeiss Sigma VP FEG SEM) and high-resolution transmission electron microscopy (HRTEM) (FEI Tecnai TF20). The structural characterizations of these microspheres were established by powder X-ray diffraction (XRD) (PANalytical X'Pert PRO MPD X-ray diffractometer) with Cu K α (λ = 1.5419 Å) as the irradiation source. The XRD pattern was obtained over the 2 θ range from 5 to 70° at 5°/min scanning rate. The N₂ sorption–desorption isotherms were recorded under liquid nitrogen (77 K) with a Micromeritics ASAP 2010 system. The CaCO₃ microparticles were degassed at 200 °C overnight prior to measurement. The surface area of the particles was calculated based on the Brunauer–Emmett–Teller (BET) equation.

2.4 Single Metal Ion Adsorption

Different concentrations of Pb²⁺, Cd²⁺, and Cu²⁺ were prepared by dissolving an appropriate mass of metal nitrate in Milli-Q water (Elix® MILLIPORE).

2.5 Effect of Contact Time

The CaCO₃ microparticles (5 mg) were mixed with 10 mL of the 50 mg/L metal ion solution. The mixtures were subject to magnetic stirring for 6 h. At different

time intervals (10, 20, 30, 60, 90, 120, 180, and 360 min), 1.2 mL of the mixture was removed and immediately centrifuged (13,500 rpm, 5 min) to pellet the microparticles. The supernatant was passed through a 0.22- μm syringe filter (FILTER-BIO, 0.22 μm), acidified with concentrated nitric acid and diluted as appropriate for inductively coupled plasma optical emission spectrometry (ICP-OES) (Optima 7000 DV, PerkinEmer) analysis to determine the metal ion concentrations.

The specific amount of heavy metal ions sequestered at different contact time, t , q_t (mg/g) was calculated by

$$q_t = \frac{(C_0 - C_t)V}{W}$$

where C_0 (mg/L) is the initial concentration of the metal ion; C_t (mg/L) is the concentration of the metal ion in the liquid phase as determined by ICP-OES after different contact times, t ; V (L) is the volume of the solution; and W (g) is the mass of adsorbent applied. This equation assumes that the volume change of the solution is negligible because the concentration of metal nitrate was small and the amount of CaCO_3 particles applied was also small (Arshadi et al. 2014).

2.6 Effect of Initial Metal Ion Concentration

The CaCO_3 microparticles (3 mg) were mixed with 6 mL of metal ion solutions in different concentrations. After stirring for 6 h, the mixture was immediately centrifuged (13,500 rpm, 5 min) to separate the solid particles from the liquid. The resulting solid was washed three times with water, air dried, sealed for further SEM and XRD study, while the supernatant was passed through a 0.22- μm syringe filter, acidified with concentrated nitric acid, and diluted as appropriate for ICP-OES analysis to determine the metal ion concentration.

The specific amount of heavy metal ions sequestered at equilibrium, q_e (mg/g), was calculated by

$$q_e = \frac{(C_0 - C_e)V}{W}$$

where C_0 (mg/L) is the initial metal ion concentration, C_e (mg/L) is the concentration in the liquid phase determined by ICP-OES at equilibrium, V (L) is the volume of the solution, and W (g) is the mass of adsorbent applied. This equation assumes that the volume change of the solution is negligible because the concentration of

metal nitrate was small and the amount of CaCO_3 particles applied was also small (Arshadi et al. 2014).

2.7 Simultaneous Adsorption of Different Heavy Metal Ions

The CaCO_3 particles (3 or 9 mg) were mixed with 6 mL of metal nitrate solution containing a combination of 50 mg/L Pb^{2+} , 50 mg/L Cd^{2+} , and 50 mg/L Cu^{2+} . The mixture was kept under magnetic stirring at room temperature for 6 h, after which time the supernatant and particles were separated by centrifugation. The resulting solid was washed three times with water and air dried before analyzing with SEM and XRD, while the supernatant was passed through a 0.22- μm syringe filter, then acidified with concentrated nitric acid and diluted as appropriate for ICP-OES analysis to determine the metal ions' concentrations.

For the investigation of the adsorption ability of activated carbon, the same procedure was followed as CaCO_3 microparticles. For the investigation of the multiple adsorbent system, 9 mg of activated carbon and 9 mg of CaCO_3 microparticles were mixed together with 6 mL of metal nitrate solution containing a combination of 50 mg/L Pb^{2+} , 50 mg/L Cd^{2+} , and 50 mg/L Cu^{2+} initially. For the investigation of the influence of proteins, the same procedure was followed; however, 9 mg of CaCO_3 particles were mixed with 6 mL of aqueous solution containing a combination of 50 mg/L Pb^{2+} , 50 mg/L Cd^{2+} , 50 mg/L Cu^{2+} , and 500 mg/L bovine serum albumin (BSA).

2.8 Possible Adsorption Mechanisms

2.8.1 Ca^{2+} Released during the Heavy Metal Adsorption

The supernatant from section “*effect of initial metal ion concentration*” was acidified by addition of concentrated nitric acid and diluted tenfold. The amount of Ca^{2+} released during the heavy metal adsorption was analyzed by ICP-OES.

2.8.2 pH Values

pH values of the metal ions solution and the supernatant after the metal ions had been adsorbed were measured using a pH meter (PHM210, MeterLab®).

3 Results and Discussion

3.1 Characterization of the CaCO₃ Micro Particles

The size and morphology of the CaCO₃ particles were visualized via SEM and HRTEM. As shown in a low-magnification SEM image (Fig. 1a), the size of the as-prepared particles is between 2 and 10 μm and most of the particles were spherical; however, several cubic-like particles were also observed. The mixture of spheres and cubic-like particles suggests the mixture of CaCO₃ polymorphs obtained to be vaterite and calcite (Wang et al. 2010b). High-magnification SEM demonstrated that the surfaces of the particles are rough, suggesting a high surface area and potentially the presence of pores (Fig. 1b). The dark center and pale edge seen under TEM, further suggested the porous nature of the particles (Fig. 1c). HRTEM confirmed the rough and porous nature of the particle surface, and it could be seen that the particles were composed of fused nanoparticles, explaining the roughness seen under SEM (Fig. 1d).

N₂ sorption–desorption experiments were carried out to quantify the porous nature and surface area of the CaCO₃ microparticles (Fig. 1e). The N₂ sorption of the CaCO₃ microparticles shows a type II isotherm, indicating that the particles are meso/macroporous particles. Specifically, the BET surface area of the CaCO₃ microparticles was 22.3 m²/g. The chemical polymorphs of the CaCO₃ microparticles were determined by powder x-ray diffraction (XRD), showing the dominate vaterite reflections, and characteristic calcite diffraction ($2\theta = 29.6^\circ$) (Fig. 1f) (Sdiri and Higashi 2013), consistent with the SEM observations.

3.2 Single-Metal Adsorption

Batch-type adsorption is a common method for investigating the adsorption ability of adsorbents. Therefore, in this study, batch-type adsorption was carried out by mixing a fixed amount of CaCO₃ microparticles (0.5 g/L) and heavy metal ion solutions with stirring (700 rpm) at room temperature (25 °C). Supersaturated metal nitrate solutions are naturally acidic, and the pH values of different species of metal nitrate solution are shown in Fig. S1.

3.3 Effect of Different Contact Time

A short equilibrium time is one of the most important characteristics for good adsorbents; therefore, the effect of different contact times was investigated in regard to the concentration of free heavy metal ions (Cu²⁺, Cd²⁺, and Pb²⁺) in the supernatant (Fig. 2a) and the percentage of heavy metal ions adsorbed by the CaCO₃ microparticles (Fig. 2b). The equilibrium was reached in a very short time (less than 10 min) for Pb²⁺ adsorption. On the other hand, it took 3 h to reach equilibrium for the removal of Cd²⁺ and of Cu²⁺. The maximum removal percentages for Pb²⁺, Cd²⁺, and Cu²⁺ were 99.9, 99.4, and 82.6%, respectively, by adding 0.5 g/L adsorbent (5 mg) to 10 mL of 50 mg/L metal ion solution. Finally, after the adsorption equilibria were established, the remaining Cu²⁺, Cd²⁺, and Pb²⁺ concentrations in the supernatant solutions were 8.7, 0.3, and 0.08 mg/L, respectively, demonstrating the remarkable ability of these porous CaCO₃ microparticles to remove Cd²⁺ and Pb²⁺ from aqueous solutions. A previous study (Sdiri et al. 2012b) also demonstrated that Pb²⁺ was adsorbed faster on CaCO₃ surfaces compared with other metal ions (e.g., Cu²⁺, Cd²⁺, and Zn²⁺), and Godelitsas et al. also found the equilibrium time for Pb²⁺ adsorbed on CaCO₃ surfaces was within 10 min (Godelitsas et al. 2003).

3.4 Effect of Different Initial Concentrations

Figure 2c, d show the effect of initial concentration on the Cu²⁺, Cd²⁺, and Pb²⁺ adsorption and the removal capacity and removal percentage are shown in Fig. 2c, d, respectively. The Pb²⁺ removal capacity increased when the initial concentration increased until the adsorption equilibrium was reached, with the maximum removal capacity for Pb²⁺ from 6 mL of solution being 1869.2 mg/g under the conditions studied. The removal capacity for Cd²⁺ from 6 mL of solution continued to increase from 99.5 to 1320.1 mg/g when the initial Cd²⁺ concentration increased from 50 to 3200 mg/L. Similarly, the removal capacity of Cu²⁺ from 6 mL of solution gradually increased from 89.3 to 105.5 mg/g when the initial Cu²⁺ concentration increased from 50 to 400 mg/L. However, when the initial Cu²⁺ concentration was 800 mg/L, the removal capacity from 6 mL of solution increased dramatically to 799.4 mg/g and increased further to 1292.5 mg/g when the initial Cu²⁺

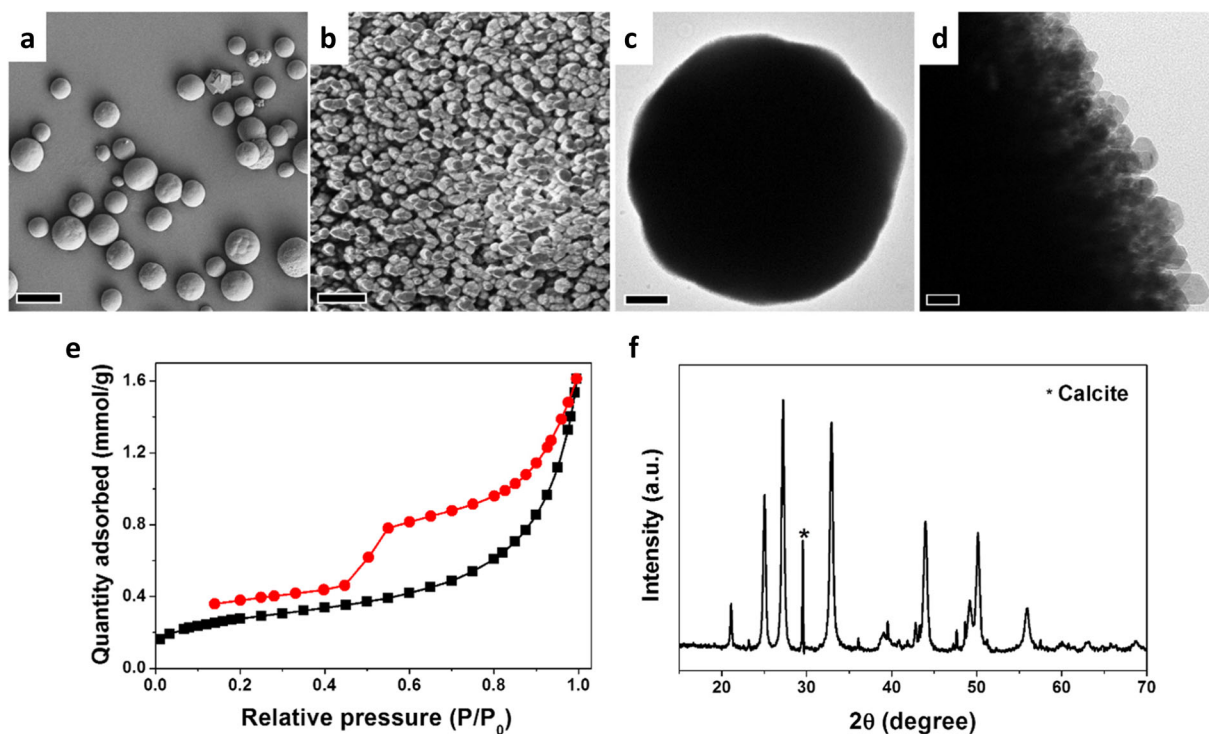


Fig. 1 Typical SEM (a, b) and TEM (c, d) images of the CaCO₃ microparticles showing the rough and porous nature of the particles. Scale bars: a 10 μm; b 200 nm; c 1 μm; and d 50 nm. N₂ sorption–desorption isotherms of the CaCO₃ microparticles (e),

concentration was 3200 mg/L. The amount of heavy metals removed from solution per unit mass of adsorbent was substantially higher than previous reports on CaCO₃ adsorption (e.g., 18.52 mg/g of Cd, 1167 mg/g of Pb and 611 mg/g of Cu) (Aziz et al. 2008; Garcia-Sánchez and Alvarez-Ayuso 2002; Hong et al. 2011; Ma et al. 2012a; Yavuz et al. 2007), which is probably due to the high surface area of the CaCO₃ microparticles.

Nearly 100% of Pb²⁺ ions were removed from the solution when the Pb²⁺ initial concentration was between 62.5 and 500 mg/L (Fig. 2d). Since the maximum amount of Pb²⁺ adsorbed on the CaCO₃ surface is constant when the adsorption equilibria are reached, as expected, when the initial Pb²⁺ concentration was increased to 4000 mg/L at the same CaCO₃ loading, the removal percentage decreased to 22.2%. Similarly, at low initial concentrations (50 and 100 mg/L), over 99.4% of Cd²⁺ was removed from the solution; however, with the CaCO₃ loading kept constant, the removal percentage kept decreasing as the initial Cd²⁺ concentration increased. This phenomenon was likely because there were not enough available adsorption sites on the

confirming the porosity of the particles. Sorption, in black; desorption, in red. The XRD pattern of representative CaCO₃ microparticles (f), demonstrating the presence of vaterite (unlabeled) and calcite (labeled) phases

CaCO₃ microparticles' surfaces when the adsorption equilibrium was reached. Notably, the removal percentage of Cu²⁺ dropped dramatically from 85.3 to 14.1% when the initial Cu²⁺ concentration increased from 50 to 400 mg/L; however, the removal percentage increased back to 51.4% when the initial concentration reached 800 mg/L, again, all at constant CaCO₃ loading. The Cu²⁺ removal percentage dropped back to 21.3% when the initial concentration was increased to 3200 mg/L. This jump in removal percentage at 800 mg/L probably occurred due to a phase transition change in the composite adsorbed material (see the “Cu²⁺ adsorption mechanisms” section). The mechanisms of Pb²⁺, Cd²⁺, and Cu²⁺ removal are discussed in the following section.

3.5 Metal Ion Adsorption Mechanisms

The heavy metal ion removal likely followed a three step process: (1) metal ion adsorption on the porous surface of the particles, (2) partial surface dissolution of the CaCO₃ particles followed by precipitation of heavy metal complexes, and (3) heavy metal complex

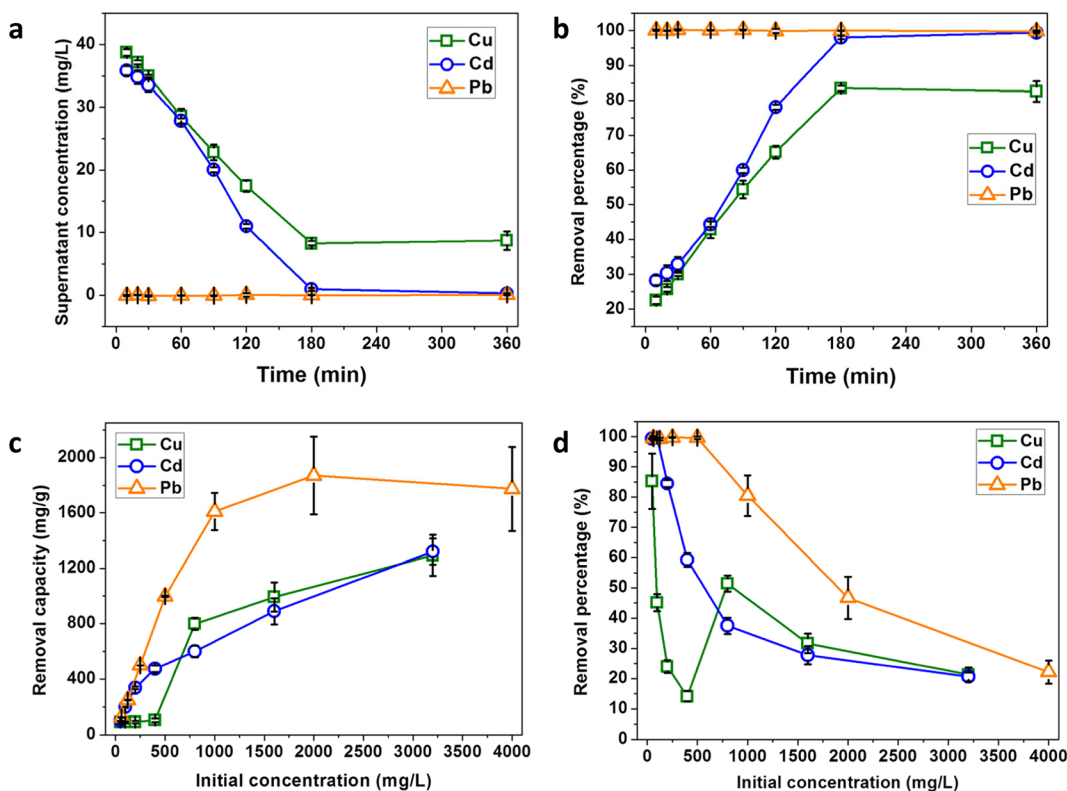
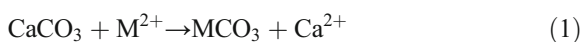


Fig. 2 Effect of different contact times on heavy metal removal by CaCO₃ microparticles: **a** remaining metal ion concentration in the supernatant and **b** removal percentage from the supernatant, with 5 mg of CaCO₃ microparticles added to 10 mL of 50 mg/L heavy

metal ions' concentrations. And effect of different initial metal ion concentrations: **c** removal capacity and **d** removal percentage, with 3 mg of CaCO₃ microparticles added to 6 mL of heavy metal ions' solutions for 6 h

nucleation and crystal growth on the CaCO₃ microparticle's surface. More specifically, firstly, the porous and negatively charged CaCO₃ microparticles (*zeta potential* -9.85 mV) would attract the positively charged heavy metal ions thereby leading to adsorption on the particles' surfaces through electrostatics. Secondly, the solubility of CaCO₃ is higher than that of the other metal carbonates involved in this study (i.e., $K_{sp}(CaCO_3) 2.8 \times 10^{-9}$, $K_{sp}(CuCO_3): 1.4 \times 10^{-10}$, $K_{sp}(CdCO_3) 5.2 \times 10^{-12}$, and $K_{sp}(PbCO_3) 7.4 \times 10^{-14}$), meaning that the higher solubility of CaCO₃ promotes some dissolution of (presumably surface) Ca²⁺ and CO₃²⁻ ions, and the lower solubility of the heavy metal carbonates leads to precipitation of a carbonate salt or mixed salt at the interface between the CaCO₃ microparticles and the metal ion solution (Eq. 1) (Pickering 1983):



Note that Eq. 1 describes the precipitation of the metal ions as their carbonate salts. The presence of

nitrate, hydroxide, and potentially other ligands will confound these equilibria, so Eq. 1 is presented only to illustrate the effects of relative solubilities on the equilibria. The amount of Ca²⁺ released and the amount of M²⁺ adsorbed were calculated (Fig. 3) and compared to see if the molar ratio of Ca²⁺ released to M²⁺ adsorbed was 1:1. Sufficient contact time was used that all systems should have been at equilibrium. Moreover, the determination of the species of metal compounds formed using XRD analysis (Fig. S2) supported the postulate that adsorption results in CaCO₃ surface dissolution and MCO₃ precipitation. Lastly, the freshly formed metal carbonates reach dissolution equilibrium in the adsorption system, and nucleation and crystal growth can occur on the surface of the CaCO₃ microparticles.

3.6 Pb²⁺ Adsorption Mechanisms

In terms of Pb²⁺ adsorption, surface dissolution and lead carbonate precipitation on the particle surfaces were the

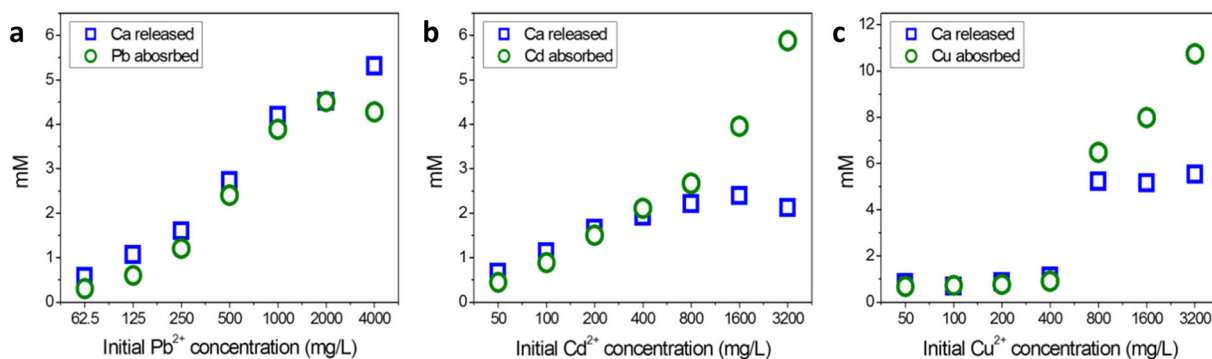
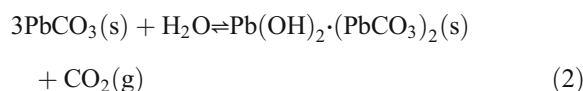


Fig. 3 The amount of Ca^{2+} released into the solution compared with the amount of heavy metal ions adsorbed: **a** Pb^{2+} , **b** Cd^{2+} , and **c** Cu^{2+} , with 3 mg of CaCO_3 microparticles added to 6 mL of heavy metal ions' solutions for 6 h

dominant mechanism, because the molar ratio of Ca^{2+} released and the Pb^{2+} adsorbed was nearly 1:1 and independent of the initial Pb^{2+} concentration up to the maximum tested (Fig. 3a). Godelitsas et al. investigated the interaction between calcium carbonates (calcite and aragonite) with Pb^{2+} in aqueous solutions by in situ atomic force microscopy (AFM) and confirmed that the adsorption of Pb^{2+} , dissolution of CaCO_3 , and the formation of lead carbonate took place in parallel until the adsorption equilibrium was reached (Godelitsas et al. 2003). However, there was some solid precipitated on the wall of the flask, especially when the initial concentration of Pb^{2+} was above 1000 mg/L, indicating the dissolution of CaCO_3 might be happening prior to the precipitation of lead carbonates because of the relative lower pH (Fig. S1A).

Two different kinds of lead carbonate compounds were observed during the Pb^{2+} adsorption process depending on the initial Pb^{2+} concentration. Namely, cerussite (PbCO_3) and hydrocerussite ($\text{Pb}_3(\text{CO}_3)_2(\text{OH})_2$; $\text{Pb}(\text{OH})_2 \cdot (\text{PbCO}_3)_2$) were observed on the surfaces of the CaCO_3 particles by SEM (Fig. 4(A2 and A4)) and XRD (Fig. S2A). The tabular, hexagonal crystals of hydrocerussite (Fig. 4(A2)) formed at low initial Pb^{2+} concentration (between 62.5 and 500 mg/L), whereas the prismatic, acicular crystals of cerussite (Fig. 4(A4)) formed at high initial Pb^{2+} concentration (2000 and 4000 mg/L). At 1000 mg/L, a mixture of cerussite and hydrocerussite was observed (see Fig. S3 for additional SEM images). Cerussite formation was also observed by HRTEM (Fig. 5). The particles obtained from the mixture after the adsorption of Pb^{2+} from a solution of initial Pb^{2+} concentration of 4000 mg/L were visualized under HRTEM, and the images show irregular particles and a crystal lattice, which was different

from that of the original porous CaCO_3 particles. XRD patterns of the particles after Pb^{2+} adsorption (Fig. S2A) further confirmed that at low initial Pb^{2+} concentrations, hydrocerussite was preferentially formed, whereas at high initial Pb^{2+} concentrations, cerussite was preferentially formed. When considering the final pH value after Pb^{2+} adsorption, it is apparent that hydrocerussite was formed under slightly basic conditions, while cerussite was formed under slightly acidic conditions (Figs. S1A and S3 for pH values and SEM image comparisons). This phenomenon was discussed by Godelitsas et al. (2003), and they claimed that the major factor for the transformation between cerussite and hydrocerussite is the pressure of CO_2 in the adsorption system (Eq. 2). Under basic conditions, there was less CO_2 in the system, and therefore hydrocerussite was more stable.



The Langmuir and Freundlich models are commonly used to describe adsorption isotherms, where the Langmuir model is based on monolayer surface adsorption, while the Freundlich model is based on surface heterogeneity with multilayer distribution of binding sites on the particles.

The Langmuir equation is expressed as

$$q_e = \frac{q_{\max} k_L C_e}{1 + k_L C_e} \quad (3)$$

Or in the linear form:

$$\frac{C_e}{q_e} = \frac{1}{q_{\max} k_L} + \frac{C_e}{q_{\max}} \quad (4)$$

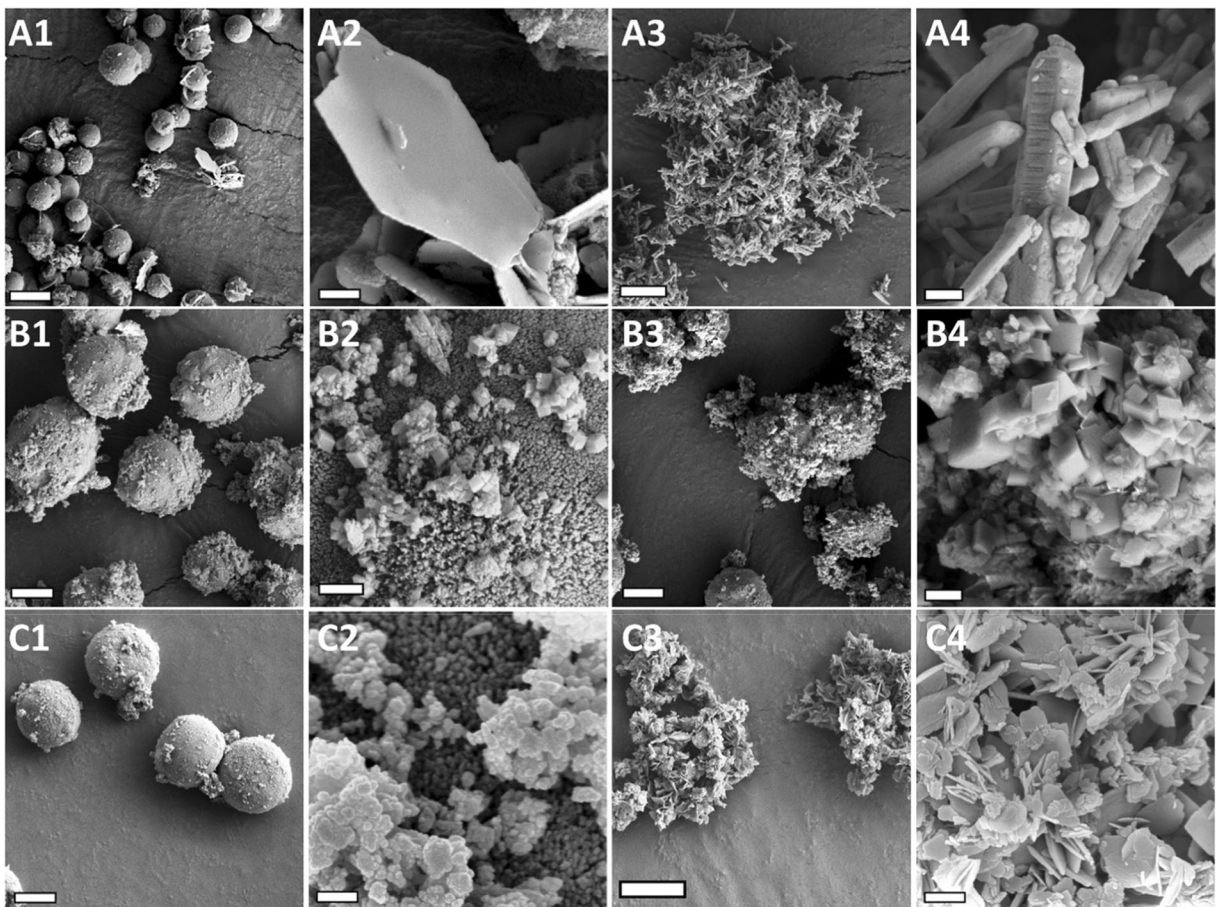


Fig. 4 SEM images of the particles after heavy metal adsorption: Pb^{2+} at 62.5 mg/L initial concentration (A1, A2) and 4000 mg/L initial concentration (A3, A4); Cd^{2+} 50 mg/L initial concentration (B1, B2) and 3200 mg/L initial concentration (B3, B4); and Cu^{2+} 50 mg/L initial concentration (C1, C2) and 3200 mg/L initial

concentration (C3, C4), with 3 mg of $CaCO_3$ particles and 6 mL of heavy metal ions' solution stirring for 6 h. Scale bars: A1, B1, C1, A3, B3, C3 5 μm ; A2, C2, C4 500 nm; A4, B4 300 nm; and A2 200 nm

where q_e is the equilibrium removal capacity (mg/g), q_{max} is the amount of heavy metal adsorbed in

a complete monolayer (mg/g), C_e is the equilibrium concentration of metal ions (mg/L), and K_L is

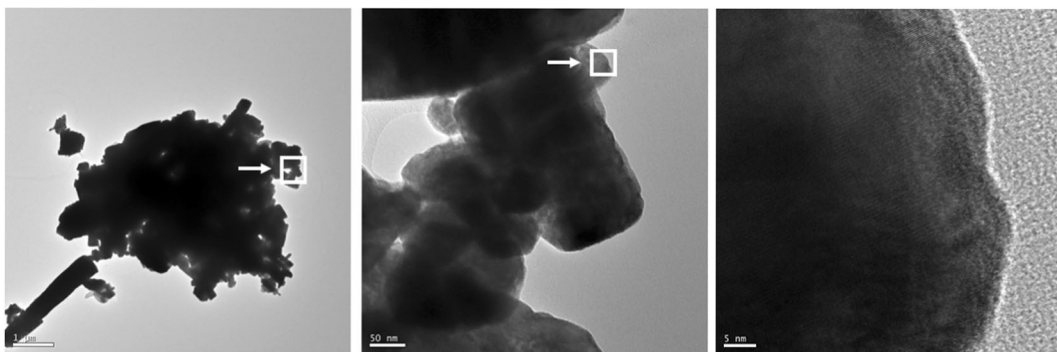


Fig. 5 HRTEM images of the particles after Pb^{2+} adsorption at 4000 mg/L

the Langmuir constant (L/mg). q_{max} and K_L can be calculated from interpretation of the slope and intercept by the linear function of C_e/q_e vs C_e .

The Freundlich equation can be expressed as

$$q_e = K_F C_e^{1/n} \quad (5)$$

Or as a linear function:

$$\ln q_e = \ln K_F + \frac{1}{n} \ln C_e \quad (6)$$

where q_e is the equilibrium removal capacity (mg/g), c_e is the equilibrium metal ion concentration in the supernatant (mg/L), K_F is the Freundlich constant, and $1/n$ is the adsorption intensity. K_F and $1/n$ can be determined from a linear plot according to Eq. 6.

The adsorption of Pb^{2+} was modeled by using both the Langmuir and the Freundlich equations. The Pb^{2+} adsorption fits the Langmuir equation better than the Freundlich equation, $R^2 = 0.9999$ and 0.8303 , respectively (Fig. 6a), suggesting that the Pb^{2+} mainly adsorbed as a monolayer on the $CaCO_3$ microparticles.

3.7 Cu^{2+} Adsorption Mechanisms

When the initial Cu^{2+} concentration was between 50 to 200 mg/L, the mechanism appeared to simply be adsorption due to the high surface area and negative charge of the $CaCO_3$ microparticles, as neither SEM (Fig. 4(C2)) nor XRD (Fig. S2B) show new crystalline compounds. Although the molar ratio of Ca^{2+} released and Cu^{2+} adsorbed was nearly 1:1 (Fig. 3c) when the initial Cu^{2+} concentration was between 50 and 200 mg/L, the surface dissolution and precipitation of $CuCO_3$ was not the adsorption mechanism. The reason for this is that the precipitation of $CuCO_3$ generally occurs above pH 6 (Sdiri and Higashi 2013); however, the final pH of the supernatant after Cu^{2+} adsorption was below 6 (Fig. S1B). When the initial Cu^{2+} concentration was 400 mg/L, flat crystals started forming on the porous $CaCO_3$ microparticle surface (Fig. S4, 400). As the initial Cu^{2+} concentration was increased above 800 mg/L, the intact $CaCO_3$ particles could barely be seen and clusters of crystals were observed on the $CaCO_3$ particles (Fig. 4(C3 and C4)), indicating that precipitation and transformation was involved at these higher concentrations. Moreover, the amount of Cu^{2+} adsorbed was much higher than the amount of Ca^{2+} released (Fig. 3c) when the initial Cu^{2+} concentration

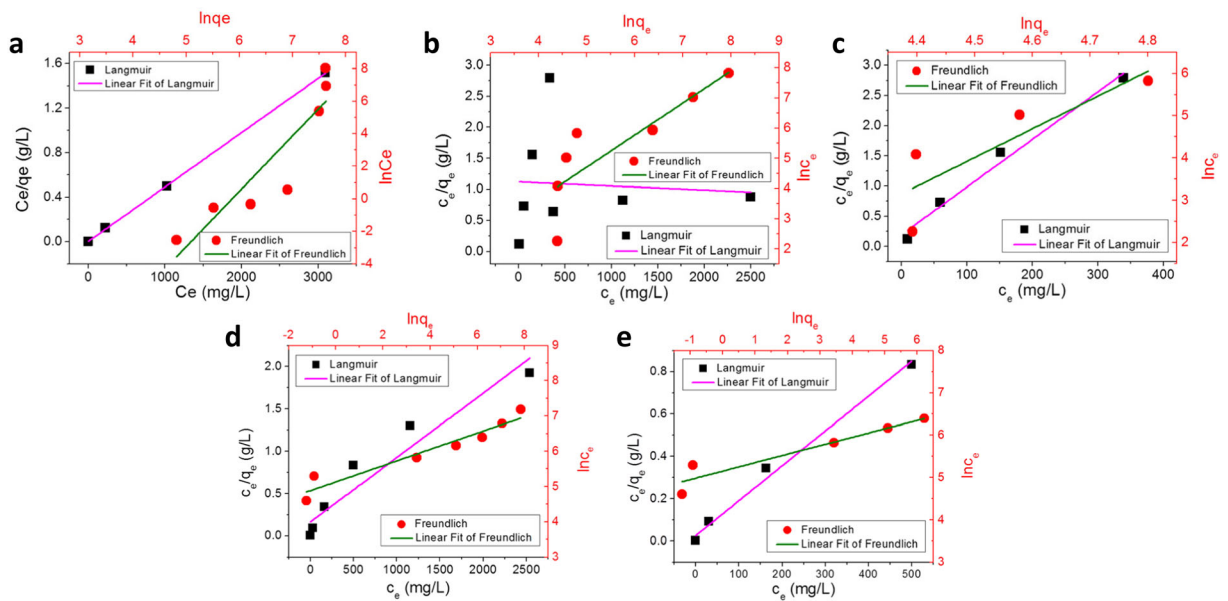


Fig. 6 Langmuir (data points in black) and Freundlich (data points in red) isotherms for **a** Pb^{2+} adsorption on porous $CaCO_3$ microparticles. For Cu^{2+} adsorption on $CaCO_3$ microparticles: **b** initial Cu^{2+} concentrations between 50 and 3200 mg/L and **c** initial

Cu^{2+} concentrations between 50 and 400 mg/L. For Cd^{2+} adsorption on $CaCO_3$ microparticles: **d** initial Cd^{2+} concentrations between 50 and 3200 mg/L and **e** initial Cd^{2+} concentrations between 50 and 800 mg/L

was above 800 mg/L. The XRD pattern of the particles (Fig. S2B) confirmed the crystals were rouaite ($\text{Cu}_2\text{NO}_3(\text{OH})_3$). We assign the phase as rouaite, rather than gerhardite, on the basis of the observation of reflections at 2θ values of 39.9, 43.6, and 49.3. The crystal structure of rouaite was reported in 1983, and rouaite was named as a mineral in 2002 by Jambor et al. (1999). It is routinely synthesized from an aqueous (2:1 mol/mol) solution of Cu^{2+} (as its nitrate) and CO_3^{2-} (Bushong and Yoder 2009). Yoder et al. discussed the synthesis pathway and solubility of rouaite in 2010 and found that rouaite is favored to form at low OH^- concentration and high NO_3^{2-} concentration. In our study, the dissolution of CaCO_3 gradually provided the OH^- and the initially added copper nitrate provided the NO_3^{2-} (Yoder et al. 2010). The K_{sp} of rouaite was found to be 10^{-36} (Yoder et al. 2010). Therefore, this crystal transformation pathway at high concentrations of Cu^{2+} could be used for large-scale removal due to the unprecedented removal capacity, easily handled precipitate, and high stability of the final material.

In order to further investigate the mechanism of Cu^{2+} adsorption, the adsorption isotherms were studied based on the Langmuir and Freundlich models. Cu^{2+} adsorption did not fit either of the adsorption assumptions when the initial concentration was between 50 and 3200 mg/L (Fig. 6b). As discussed above, Cu^{2+} adsorption may have different adsorption mechanisms at different initial Cu^{2+} concentrations, and therefore, the Langmuir and Freundlich models were used for initial concentrations of Cu^{2+} between 50 and 400 mg/L (Fig. 6c). Cu^{2+} adsorption between 50 and 400 mg/L fits the Langmuir model better (Fig. 6b, $R^2 = 0.9846$) than it does the Freundlich model (Fig. 6c, $R^2 = 0.7311$), suggesting that monolayer adsorption was the major adsorption mechanism for Cu^{2+} adsorption in the initial concentration range of 50–400 mg/L.

3.8 Cd^{2+} Adsorption Mechanisms

The amount of Ca^{2+} released to the supernatant was similar to the amount of Cd^{2+} adsorbed between the initial concentrations of 50 and 800 mg/L (Fig. 3b). However, the amount of Cd^{2+} adsorbed was significantly higher than the amount of Ca^{2+} released when the initial Cd^{2+} concentrations were above 800 mg/L (Fig. 3b). A microcrystal morphology with flat surfaces and sharp angles was imaged by SEM after adsorbing Cd^{2+} on the CaCO_3 particles at low and high initial Cd^{2+}

concentrations (Fig. 4(B2 and B4)). However, the size of the crystals was much larger at higher initial Cd^{2+} concentrations compared to the lower initial Cd^{2+} concentrations. The XRD patterns confirmed that the crystals were otavite (CdCO_3) (Fig. S2C), indicating that the mechanism of Cd^{2+} adsorption on CaCO_3 porous microparticles was mainly surface dissolution and precipitation/transformation. At high initial concentrations (1600 and 3200 mg/L), the amount of Cd^{2+} adsorbed was significantly higher than the amount of Ca^{2+} released, which was likely because the high surface area and negative charge of the CaCO_3 microparticles allowed for the adsorption of Cd^{2+} on the surface in parallel with the surface dissolution of Ca^{2+} and subsequent CdCO_3 precipitation. The fits to the Langmuir and Freundlich models helped confirm these mechanistic insights.

When investigating the adsorption isotherms for the whole range of initial Cd^{2+} concentrations (from 50 to 3200 mg/L), the R^2 values from the fit to the Langmuir and Freundlich models were 0.9268 and 0.9318, respectively, highlighting the similarities between these two assumptions for Cd^{2+} adsorption (Fig. 6d). However, when considering the initial Cd^{2+} concentrations between 50 and 800 mg/L (similar moles of Cd^{2+} adsorbed and Ca^{2+} released according to Fig. 3b), the adsorption fits more closely with the Langmuir model ($R^2 = 0.9918$) than with the Freundlich model ($R^2 = 0.9048$) (Fig. 6e). These results at lower initial Cd^{2+} concentrations suggested that there was monolayer adsorption at low concentrations and multilayer adsorption at high concentrations.

3.9 Simultaneous Adsorption of Multiple Heavy Metals

The competitive and selective adsorption among Cu^{2+} , Cd^{2+} , and Pb^{2+} was carried out with 0.5 and 1.5 g/L CaCO_3 microparticles added to solutions containing all three metal ions (each at a concentration of 50 mg/L), and the adsorption efficiency was compared with single metal adsorption at the same individual metal ion concentration of 50 mg/L (Table 2). In the multiple metal system, the amount of CaCO_3 microparticles significantly affected the heavy metal removal efficiency. Thus, a series of experiments was conducted with the same amount of CaCO_3 microparticles used for the individual metal ion adsorption studies, and a second series of experiments used three times that amount of CaCO_3 , so that, in this latter case, the mass ratio of

CaCO₃ microparticles to total metal ion amounts equaled that for the experiments using individual metal ions. With the lower relative amount of CaCO₃ microparticles, the metal ion removal efficiencies were, perhaps not unexpectedly, less than observed for the individual metal ions. When using the increased quantity of CaCO₃ particles, such that the mass ratio of CaCO₃ microparticles to total metal ions was that used for studying the individual metal ions, the removal efficiency for Cu²⁺, Cd²⁺, and Pb²⁺ increased to 109.0, 56.1, and 98.6%, respectively (Table 2, entry 2 vs entry 3). Since 0.5 g/L of the CaCO₃ microparticles were added to the single metal system, the total quantity of CaCO₃ microparticles used for all three different metal ions corresponded to 1.5 g/L. Therefore, the rest of the discussion focusses on the experiments utilizing 1.5 g/L CaCO₃ microparticles as adsorbents for the multiple metal system (Table 2, entry 3).

In the multiple metal system, the concentration of Cu²⁺ in the supernatant after adsorption was lower than the detection limit of the ICO-OES instrument; therefore, a value of 100% is claimed for Cu²⁺ removal. When all three metals were present, the Cd²⁺ adsorption was significantly inhibited, likely due to competition, while the Cu²⁺ adsorption was promoted compared with the single metal systems (Table 2, entry 1 vs entry 3). On the other hand, the Pb²⁺ adsorption capacity was relatively unchanged between the two systems. Normally, different degrees of inhibition are seen in adsorption systems with multiple elements when compared against single element adsorption systems (Ren et al. 2017; Saha et al. 2016; Sdiri et al. 2012a). The reason that Cu²⁺ adsorption was promoted in the multiple metal system in this study (from 82.6 to 100%) could be due to co-precipitation in the complicated system or could

be because the slightly basic final pH (7.5) promoted the formation of copper complexes of some combination of hydroxide and carbonate ligands. The relatively minimal decrease in Pb²⁺ adsorption (97.5% in the multiple metal system vs 99.9% for the single metal system) was probably due to a slight decrease in the available adsorption sites on the CaCO₃ particle surface. Additionally, this minimal decrease demonstrates that neither Cu²⁺ nor Cd²⁺ inhibit Pb²⁺ adsorption.

Although 99.4% of Cd²⁺ can be removed from the single-metal system (Table 2, entry 1), which is often ascribed to the similar hydrated ionic radius of Cd²⁺ and Ca²⁺ (0.99 and 0.97 Å, respectively) allowing for simple replacement, this hypothesis does not necessarily apply under competitive binding scenarios such as the multiple metal system investigated in this study. Sidiri and Higashi investigated the adsorption of ternary and quadruple systems of Cu²⁺, Cd²⁺, Pb²⁺, and Zn²⁺ by natural limestone samples, and also found that Cd²⁺ adsorption was greatly inhibited in the presence of Pb²⁺. This suggests that synthetic CaCO₃ microparticles behave similarly to natural limestone in some regards.

More complex aqueous systems with proteins present were also tested (Table 2, entry 4). In the presence of bovine serum albumin (BSA), the adsorption capacity of all three metal ions studied was significantly inhibited: the removal capacity of Cu²⁺ was reduced from 100 to 79.5%; Cd²⁺ was reduced from 37 to 0%, and Pb²⁺ was reduced from 97.5 to 77.8%, respectively (Table 2, entry 3 vs entry 4). As activated carbon is a common heavy metal adsorbent, the adsorption capacity of multiple metal ions was also compared against activated carbon (Table 2, entry 5), and the mixture of activated carbon and CaCO₃ microparticles as co-adsorbents was also studied to determine whether

Table 2 Comparison of the removal efficiency between single-element adsorption and multiple-element adsorption

Metal system	Adsorbent (g/L)	Adsorbent type	Removal efficiency (%)		
			Cu ²⁺	Cd ²⁺	Pb ²⁺
Single metal	0.5	CaCO ₃	82.6	99.4	99.9
Multiple metals	0.5	CaCO ₃	47.9	23.7	49.1
Multiple metals	1.5	CaCO ₃	100	37.0	97.5
Multiple metals + BSA	1.5	CaCO ₃	79.5	0	77.8
Multiple metals	1.5	Activated carbon	40.0	0	34.1
Multiple metals	1.5 + 1.5	Activated carbon and CaCO ₃	94.5	11.0	89.5

BSA bovine serum albumin

synergistic adsorption effects exist (Table 2, entry 6). The adsorption efficiency of activated carbon was low (40.0% of Cu^{2+} , 0% of Cd^{2+} , and 34.1% of Pb^{2+}) (Table 2, entry 5). The multiple-adsorbent system did increase the adsorption efficiency compared to the activated carbon (Table 2, entry 6 vs entry 5) but decreased the adsorption efficiency compared with CaCO_3 microparticles by themselves (Table 2, entry 6 vs entry 3).

4 Conclusion

Porous CaCO_3 microparticles were prepared successfully by a rapid precipitation reaction and were applied to heavy metal ion removal from aqueous media. These particles were found to be highly effective in removing large quantities of toxic heavy metal ions from both single-metal and multiple metal systems due to the high surface area and negative charge of the particles and higher solubility of CaCO_3 compared with the heavy metal carbonates that form during adsorption. Importantly, compared with other possible adsorbents, these CaCO_3 microparticles are low cost, easy to scale up, and potentially can be applied for the large-scale sequestration and facile recovery of industrial heavy metal ions contaminating wastewater.

Acknowledgements R. Zhang thanks the University of Sydney for a scholarship for her PhD study and the scientific and technical assistance, of the Australian Centre for Microscopy and Microanalysis (ACMM) Research Facility at the University of Sydney. Dr. Alexander K.Y. Yuen is acknowledged for his assistance with N_2 sorption–desorption isotherm analysis. Dr. Shane Wilkinson is acknowledged for his support of ICP-OES analysis. Dr. Kang Liang acknowledges the support from the Scientia Fellowship program at UNSW.

References

- Al-Rashdi, B., Johnson, D., & Hilal, N. (2013). Removal of heavy metal ions by nanofiltration. *Desalination*, 315, 2–17.
- Amuda, O., Giwa, A., & Bello, I. (2007). Removal of heavy metal from industrial wastewater using modified activated coconut shell carbon. *Biochemical Engineering Journal*, 36, 174–181.
- Annadurai, G., Juang, R., & Lee, D. (2003). Adsorption of heavy metals from water using banana and orange peels. *Water Science and Technology*, 47, 185–190.
- Arshadi, M., Amiri, M., & Mousavi, S. (2014). Kinetic, equilibrium and thermodynamic investigations of Ni (II), Cd (II), Cu (II) and Co (II) adsorption on barley straw ash. *Water Resources and Industry*, 6, 1–17.
- Aziz, H. A., Adlan, M. N., & Ariffin, K. S. (2008). Heavy metals (Cd, Pb, Zn, Ni, Cu and Cr (III)) removal from water in Malaysia: post treatment by high quality limestone. *Bioresource Technology*, 99, 1578–1583.
- Blöcher, C., Dorda, J., Mavrov, V., Chmiel, H., Lazaridis, N., & Matis, K. (2003). Hybrid flotation-membrane filtration process for the removal of heavy metal ions from wastewater. *Water Research*, 37, 4018–4026.
- Boparai, H. K., Joseph, M., & O'Carroll, D. M. (2011). Kinetics and thermodynamics of cadmium ion removal by adsorption onto nano zerovalent iron particles. *Journal of Hazardous Materials*, 186, 458–465.
- Bushong, E. J., & Yoder, C. H. (2009). The synthesis and characterization of rouaite, a copper hydroxy nitrate. An integrated first-year laboratory project. *Journal of Chemical Education*, 86, 80.
- Cai, G. B., Zhao, G. X., Wang, X. K., & Yu, S. H. (2010). Synthesis of polyacrylic acid stabilized amorphous calcium carbonate nanoparticles and their application for removal of toxic heavy metal ions in water. *The Journal of Physical Chemistry C*, 114, 12948–12954.
- Celis, R., Hermosin, M. C., & Cornejo, J. (2000). Heavy metal adsorption by functionalized clays. *Environmental Science & Technology*, 34, 4593–4599.
- Charemtanyarak, L. (1999). Heavy metals removal by chemical coagulation and precipitation. *Water Science and Technology*, 39, 135–138.
- Erdem, E., Karapinar, N., & Donat, R. (2004). The removal of heavy metal cations by natural zeolites. *Journal of Colloid and Interface Science*, 280, 309–314.
- Fu, F., & Wang, Q. (2011). Removal of heavy metal ions from wastewaters: a review. *Journal of Environmental Management*, 92, 407–418.
- Gamsjäger, H., Fluch, A., & Swinehart, J. H. (1984). The effect of potential aqueous pollutants on the solubility of Pb^{2+} in cerussite-calcite phase. *Monatshfte für Chemie/Chemical Monthly*, 115, 251–259.
- García-Sánchez, A., & Alvarez-Ayuso, E. (2002). Sorption of Zn, Cd and Cr on calcite. Application to purification of industrial wastewaters. *Minerals Engineering*, 15, 539–547.
- Godelitsas, A., Astilleros, J. M., Hallam, K., Harissopoulos, S., & Putnis, A. (2003). Interaction of calcium carbonates with lead in aqueous solutions. *Environmental Science & Technology*, 37, 3351–3360.
- Gupta, V. K., Agarwal, S., & Saleh, T. A. (2011). Synthesis and characterization of alumina-coated carbon nanotubes and their application for lead removal. *Journal of Hazardous Materials*, 185, 17–23.
- Ho, Y. S., Wase, D. J., & Forster, C. (1996). Kinetic studies of competitive heavy metal adsorption by sphagnum moss peat. *Environmental Technology*, 17, 71–77.
- Hong, K. S., Lee, H. M., Bae, J. S., Ha, M. G., Jin, J. S., Hong, T. E., Kim, J. P., & Jeong, E. D. (2011). Removal of heavy metal ions by using calcium carbonate extracted from starfish treated by protease and amylase. *Journal of Analytical Science and Technology*, 2, 75–82.
- Hua, M., Zhang, S., Pan, B., Zhang, W., Lv, L., & Zhang, Q. (2012). Heavy metal removal from water/wastewater by

- nanosized metal oxides: a review. *Journal of Hazardous Materials*, 211, 317–331.
- Jambor, J. L., Puziewicz, J., & Roberts, A. C. (1999). New mineral names. *American Mineralogist*, 84, 685–688.
- Kobyas, M., Demirbas, E., Senturk, E., & Ince, M. (2005). Adsorption of heavy metal ions from aqueous solutions by activated carbon prepared from apricot stone. *Bioresource Technology*, 96, 1518–1521.
- Lin, S. H., Lai, S. L., & Leu, H. G. (2000). Removal of heavy metals from aqueous solution by chelating resin in a multi-stage adsorption process. *Journal of Hazardous Materials*, 76, 139–153.
- Ma, X., Li, L., Yang, L., Su, C., Wang, K., & Jiang, K. (2012a). Preparation of hybrid CaCO₃-pepsin hemisphere with ordered hierarchical structure and the application for removal of heavy metal ions. *Journal of Crystal Growth*, 338, 272–279.
- Ma, X., Li, L., Yang, L., Su, C., Wang, K., Yuan, S., & Zhou, J. (2012b). Adsorption of heavy metal ions using hierarchical CaCO₃-maltose meso/macroporous hybrid materials: adsorption isotherms and kinetic studies. *Journal of Hazardous Materials*, 209, 467–477.
- Matlock, M. M., Howerton, B. S., & Atwood, D. A. (2002). Chemical precipitation of heavy metals from acid mine drainage. *Water Research*, 36, 4757–4764.
- Mohammadifard, H., & Amiri, M. C. (2017). Evaluating Cu (II) removal from aqueous solutions with response surface methodology by using novel synthesized CaCO₃ nanoparticles prepared in a colloidal gas aphon system. *Chemical Engineering Communications*, 204, 476–484.
- Okoye, A., Ejikeme, P., & Onukwuli, O. (2010). Lead removal from wastewater using fluted pumpkin seed shell activated carbon: adsorption modeling and kinetics. *International Journal of Environmental Science & Technology*, 7, 793–800.
- Pickering, W. (1983). Extraction of copper, lead, zinc or cadmium ions sorbed on calcium carbonate. *Water, Air, & Soil Pollution*, 20, 299–309.
- Reed, B. E., & Matsumoto, M. R. (1993). Modeling cadmium adsorption by activated carbon using the Langmuir and Freundlich isotherm expressions. *Separation Science and Technology*, 28, 2179–2195.
- Ren, C., Ding, X., Li, W., Wu, H., & Yang, H. (2017). Highly efficient adsorption of heavy metals onto novel magnetic porous composites modified with amino groups. *Journal of Chemical & Engineering Data*, 62, 1865–1875.
- Ricco, R., Konstas, K., Styles, M. J., Richardson, J. J., Babarao, R., Suzuki, K., Scopece, P., & Falcaro, P. (2015). Lead (II) uptake by aluminium based magnetic framework composites (MFCs) in water. *Journal of Materials Chemistry A*, 3, 19822–19831.
- Richardson, J. J., Maina, J. W., Ejima, H., Hu, M., Guo, J., Choy, M. Y., Gunawan, S. T., Lybaert, L., Hagemeyer, C. E., & De Geest, B. G. (2015). Versatile loading of diverse cargo into functional polymer capsules. *Advanced Science*, 2, 1400007.
- Saha, D., Barakat, S., Van Bramer, S. E., Nelson, K. A., Hensley, D. K., & Chen, J. (2016). Noncompetitive and competitive adsorption of heavy metals in sulfur-functionalized ordered mesoporous carbon. *ACS Applied Materials & Interfaces*, 8, 34132–34142.
- Sdiri, A., & Higashi, T. (2013). Simultaneous removal of heavy metals from aqueous solution by natural limestones. *Applied Water Science*, 3, 29–39.
- Sdiri, A., Higashi, T., Chaabouni, R., & Jamoussi, F. (2012a). Competitive removal of heavy metals from aqueous solutions by montmorillonitic and calcareous clays. *Water, Air, & Soil Pollution*, 223, 1191–1204.
- Sdiri, A., Higashi, T., Jamoussi, F., & Bouaziz, S. (2012b). Effects of impurities on the removal of heavy metals by natural limestones in aqueous systems. *Journal of Environmental Management*, 93, 245–253.
- Srivastava, V. C., Mall, I. D., & Mishra, I. M. (2006). Equilibrium modelling of single and binary adsorption of cadmium and nickel onto bagasse fly ash. *Chemical Engineering Journal*, 117, 79–91.
- Stafiej, A., & Pyrzyńska, K. (2007). Adsorption of heavy metal ions with carbon nanotubes. *Separation and Purification Technology*, 58, 49–52.
- Tavakoli, O., Goodarzi, V., Saeb, M. R., Mahmoodi, N. M., & Borja, R. (2017). Competitive removal of heavy metal ions from squid oil under isothermal condition by CR11 chelate ion exchanger. *Journal of Hazardous Materials*, 334, 256–266.
- Wang, X., Cai, W., Lin, Y., Wang, G., & Liang, C. (2010a). Mass production of micro/nanostructured porous ZnO plates and their strong structurally enhanced and selective adsorption performance for environmental remediation. *Journal of Materials Chemistry*, 20, 8582–8590.
- Wang, Y., Moo, Y. X., Chen, C., Gunawan, P., & Xu, R. (2010b). Fast precipitation of uniform CaCO₃ nanospheres and their transformation to hollow hydroxyapatite nanospheres. *Journal of Colloid and Interface Science*, 352, 393–400.
- Wang, Z., Feng, Y., Hao, X., Huang, W., & Feng, X. (2014). A novel potential-responsive ion exchange film system for heavy metal removal. *Journal of Materials Chemistry A*, 2, 10263–10272.
- Yavuz, O., Guzel, R., Aydin, F., Tegin, I., & Ziyadanogullari, R. (2007). Removal of cadmium and lead from aqueous solution by calcite. *Polish Journal of Environmental Studies*, 16, 467.
- Yoder, C., Bushong, E., Liu, X., Weidner, V., McWilliams, P., Martin, K., Lorgunpai, J., Haller, J., & Schaeffer, R. (2010). The synthesis and solubility of the copper hydroxyl nitrates: gerhardtite, rouaite and likasite. *Mineralogical Magazine*, 74, 433–440.